Geoscience Frontiers 5 (2014) 673–682

Contents lists available at ScienceDirect

China University of Geosciences (Beijing)

Geoscience Frontiers

journal homepage: www.elsevier.com/locate/gsf

Research paper

Fluid-rock interaction in retrograde granulites of the Southern Marginal Zone, Limpopo high grade terrain, South Africa

Jan Marten Huizenga [a,b,*], Dirk van Reenen [c], Jacques L.R. Touret [d]

[a] Unit of Environmental Sciences and Management, North-West University, Private Bag X6001, 2520, South Africa
[b] Economic Geology Research Institute (EGRU), School of Earth and Environmental Sciences, James Cook University, Townsville, QLD 4811, Australia
[c] Department of Geology, University of Johannesburg, Johannesburg, South Africa
[d] Institut de Minéralogie, de Physique des Matériaux, et de Cosmochimie (IMPMC) Sorbonne Universités – UPMC Univ Paris 06, UMR CNRS 7590, Muséum National d'Histoire Naturelle, IRD UMR 206, 4 Place Jussieu, F-75005

ARTICLE INFO

Article history:
Received 31 August 2013
Received in revised form
4 January 2014
Accepted 9 January 2014
Available online 4 February 2014

Keywords:
Granulite
Fluid
Limpopo
Retrograde
Southern Marginal Zone

ABSTRACT

Fluid infiltration into retrograde granulites of the Southern Marginal Zone (Limpopo high grade terrain) is exemplified by hydration reactions, shear zone hosted metasomatism, and lode gold mineralisation. Hydration reactions include the breakdown of cordierite and orthopyroxene to gedrite + kyanite, and anthophyllite, respectively. Metamorphic petrology, fluid inclusions, and field data indicate that a low H_2O-activity carbon-saturated CO_2-rich and a saline aqueous fluid infiltrated the Southern Marginal Zone during exhumation. The formation of anthophyllite after orthopyroxene established a regional retrograde anthophyllite-in isograd and occurred at *P-T* conditions of ~6 kbar and 610 °C, which fixes the minimum mole fraction of H_2O in the CO_2-rich fluid phase at ~0.1. The maximum H_2O mole fraction is fixed by the lower temperature limit (~800 °C) for partial melting at ~0.3. C-O-H fluid calculations show that the CO_2-rich fluid had an oxygen fugacity that was 0.6 $\log_{10}$ units higher than that of the fayalite-magnetite-quartz buffer and that the $CO_2/(CO_2+CH_4)$ mole ratio of this fluid was 1. The presence of dominantly relatively low density CO_2-rich fluid inclusions in the hydrated granulites indicates that the fluid pressure was less than the lithostatic pressure. This can be explained by strike slip faulting and/or an increase of the rock permeability caused by hydration reactions.

1. Introduction

The Limpopo high-grade terrain in South Africa is well known for its classic exposures of regionally metamorphosed granulite-facies rocks. It is a late Archean ENE–WSW trending zone located between the granite-greenstone terrains of the Zimbabwe and Kaapvaal cratons (Fig. 1), subdivided into the Northern Marginal Zone, the Central Zone, and the Southern Marginal Zone (e.g., Van Reenen et al., 2011). The Northern and Southern Marginal Zones comprise high-grade granitoids and greenstone belt lithologies (e.g., Kreissig et al., 2001; Van Reenen et al., 2011), which are juxtaposed against the cratons as a result of compression-related exhumation in the interval ~2.69–2.62 Ga (Van Reenen et al., 2011).

The Southern Marginal Zone (SMZ) is particularly interesting as its metamorphic evolution is typical for subduction-related high-pressure granulites (clockwise *P-T* path), which also experienced ultrahigh-temperature conditions (Tsunogae et al., 2004; Belyanin et al., 2012). Granulites that show a clockwise *P-T* path and experienced both high-pressure and ultrahigh temperature conditions are not common (Touret and Huizenga, 2012). Further, the SMZ shows evidence of both near-peak and retrograde fluid-rock interaction during thrust-controlled exhumation in the interval 2.69–2.62 Ga (Van Reenen et al., 2011). The limit of the regionally retrogressed granulite corresponds to a rarely described retrograde

* Corresponding author. James Cook University, Economic Geology Research Institute, School of Earth and Environmental Sciences, Townsville, QLD 4811, Australia.
E-mail address: jan.huizenga@jcu.edu.au (J.M. Huizenga).

Peer-review under responsibility of China University of Geosciences (Beijing)

Production and hosting by Elsevier

1674-9871/$ – see front matter © 2014, China University of Geosciences (Beijing) and Peking University. Production and hosting by Elsevier B.V. All rights reserved.
http://dx.doi.org/10.1016/j.gsf.2014.01.004

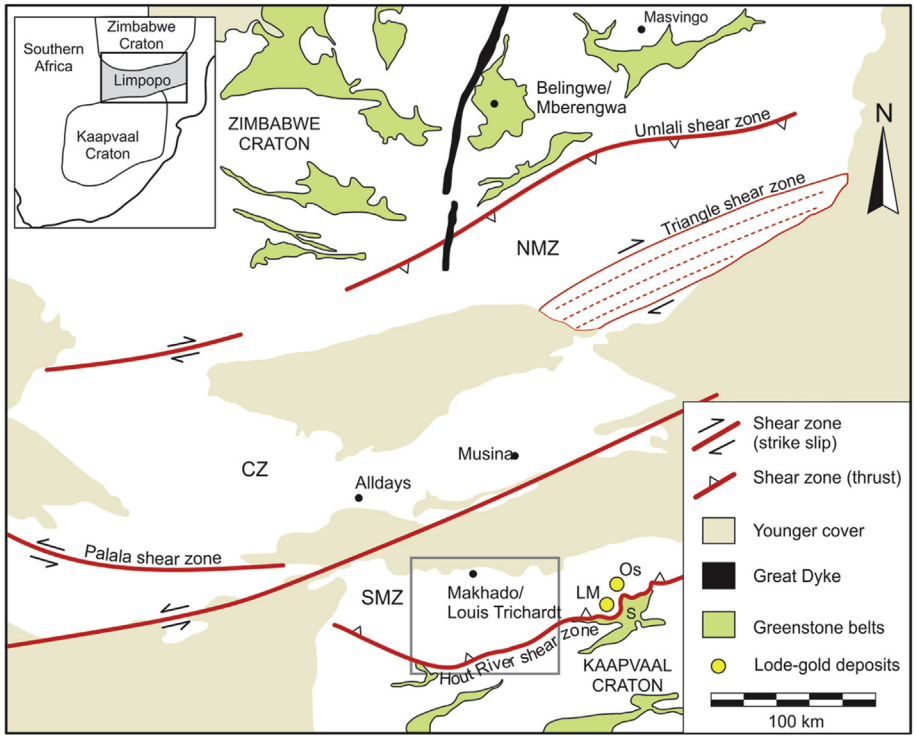

Figure 1. Geological map of the Limpopo high-grade terrain and the adjacent Kaapvaal and Zimbabwe cratons (modified after Rollinson, 1993). SMZ: Southern Marginal Zone, CZ: Central Zone, NMZ: Northern Marginal Zone, S: Sutherland/Giyani greenstone belt, LM: Louis Moore gold deposit, Os: Osprey gold deposit. Inset: see Fig. 2.

anthophyllite-in isograd (Van Reenen, 1986). The SMZ is thus an ideal terrain where the physico-chemical effects of fluid-rock interaction at deep- and mid-crustal levels can be studied.

The emphasis of this paper is to demonstrate the importance of an integrated approach of field mapping, mineralogy, fluid inclusion studies, and thermodynamic modelling in studying different aspects (i.e., *P*, *T*, fluid composition and redox state) of fluid-rock interaction in cooling granulites. We reviewed and reinterpreted mineralogical and fluid inclusions data from the literature, and applied thermodynamic model calculations within the C-O-H fluid system.

2. Geological setting of the Southern Marginal Zone

The SMZ is subdivided into a granulite zone (comprising garnet-orthopyroxene-cordierite-bearing metapelitic lithologies) in the north and a retrograde hydrated granulite zone (comprising garnet-biotite-plagioclase-anthophyllite ± gedrite ± kyanite-bearing lithologies) in the south (e.g., Van Reenen, 1986; Van Reenen et al., 2011) (Fig. 2). These two zones are chemically equivalent (Kreissig et al., 2000) and separated by the retrograde anthophyllite-in isograd (Van Reenen, 1986). Migmatitic pelitic rocks in the granulite zone show reaction textures that are associated with decompression and cooling from peak conditions at $P > 10$ kbar and $T = \sim 1000$ °C (e.g., Tsunogae et al., 2004; Van Reenen et al., 2011; Belyanin et al., 2012). They are characterised by the following four mineral assemblages: (1) orthopyroxene-plagioclase-biotite-quartz (±garnet, ±K-feldspar), (2) garnet-orthopyroxene-plagioclase-biotite-quartz (±K-feldspar), (3) garnet-orthopyroxene-cordierite-plagioclase-biotite-quartz (±K-feldspar), and (4) orthopyroxene-cordierite-plagioclase-biotite-quartz (±K-feldspar) (e.g., Van Reenen et al., 2011). Mineral assemblages (3) and (4) formed as a result of the reaction:

$$\underset{\text{Garnet}}{2(Fe,Mg)_3Al_2Si_3O_{12}} + \underset{\text{Quartz}}{3\ SiO_2} \rightarrow \underset{\text{Orthopyroxene}}{2(Fe,\ Mg)_2Si_2O_6} + \underset{\text{Cordierite}}{(Fe,Mg)_2Al_4Si_5O_{18}} \quad (1)$$

during decompression and cooling (e.g., Van Reenen et al., 2011). Iron-rich rocks with a Mg/(Mg + Fe) mole ratio < 0.6 do not show any sign of reaction (1) whereas this reaction has run to completion in rocks with a Mg/(Mg + Fe) mole ratio > 0.7 (Van Reenen, 1986). Rocks with a Mg/(Mg + Fe) mole ratio between 0.6 and 0.7 show reaction (1) in progress (Fig. 3a) (Van Reenen, 1986).

The rare occurrence of primary mixed saline H_2O-CO_2 fluid inclusions in orthopyroxene (Touret and Huizenga, 2011) and in quartz inclusions in garnet (Van den Berg and Huizenga, 2001) indicates that granulite facies metamorphism occurred in the presence of a CO_2 and a saline aqueous fluid (Van den Berg and Huizenga, 2001; Touret and Huizenga, 2011). These low-H_2O activity fluids coexisted under conditions of immiscibility and are considered to be typical granulite facies fluids (e.g., Newton et al., 1998).

Post-peak grain-size scale metasomatism is exemplified by perthitic feldspar rims between quartz and garnet, which is the result of the reaction Garnet + Quartz + $(K,Na)_{fluid}$ → K-feldspar + Albite + Biotite (Touret and Huizenga, 2011). Large-scale, shear zone related metasomatism is shown by potassium alteration of tonalitic orthopyroxene-bearing gneisses in the Petronella Shear Zone (Fig. 2) (Smit and Van Reenen, 1997). Here, mesoperthite, perthite, and antiperthite are replacing precursor oligoclase (Smit and Van Reenen, 1997) while orthopyroxene remains stable. Whole-rock/garnet/quartz oxygen-isotope fractionation of the metasomatosed rocks

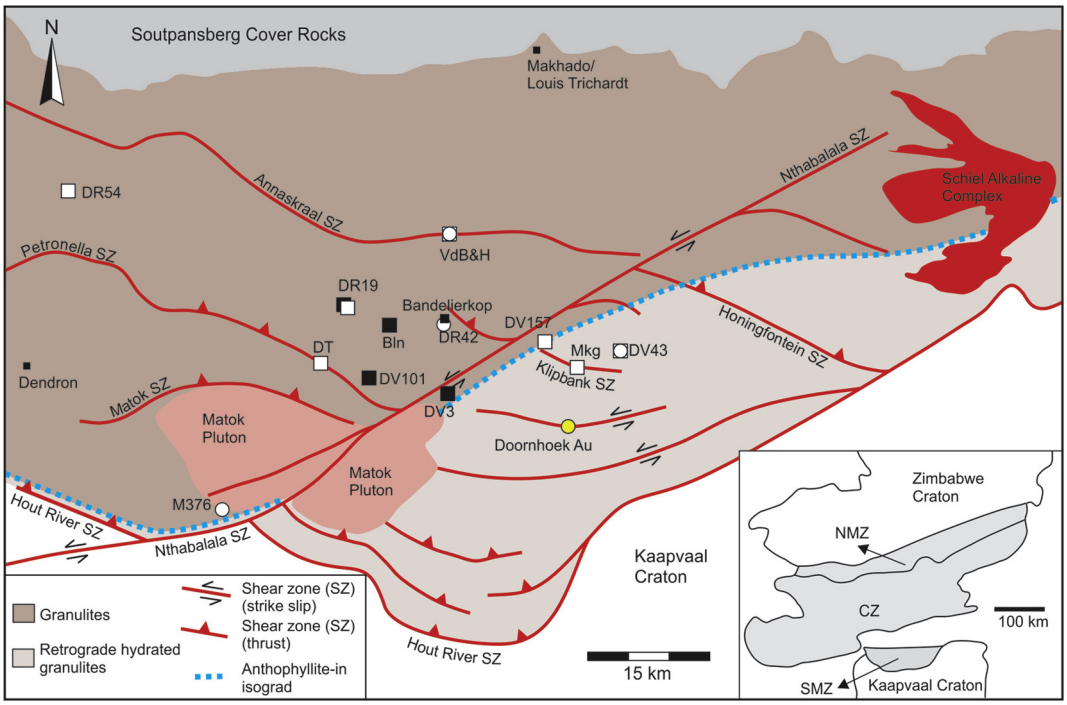

Figure 2. Geological map of the Southern Marginal Zone of the Limpopo high-grade terrain (modified after Smit and Van Reenen, 1997). Black squares indicate sample localities of samples that were used for *P-T* reconstruction by Perchuk et al. (2000b) (sample localities: DR19, DV101, DV3) and Belyanin et al. (2012) (sample locality: Bln). White squares represent localities of samples that were used for fluid inclusion studies by Van Reenen and Hollister (1988) (sample localities: DR54, DR19, DR157, DV43), Du Toit (1994) (sample locality: DT), Mokgatlha (1995) (sample locality: Mkg) and Van den Berg and Huizenga (2001) (sample locality: VdB&H). White circles indicate localities of samples of which fluid inclusion microphotographs/sketch are shown in Fig. 4 (sample localities: VdB&H, DV43, DR42).

indicates that alteration took place at a temperature >800 °C (Hoernes et al., 1995; Smit and Van Reenen, 1997). Both the grain-size scale and large-scale metasomatic features indicate that a post-peak metamorphic high-salinity fluid was present.

3. Retrograde hydration and metasomatism in the southern part of the SMZ

Retrogradation of Mg-rich, K-poor pelitic and tonalitic granulites in the presence of H_2O-bearing fluid phase resulted in hydration of cordierite and orthopyroxene (Van Reenen, 1986; Van Reenen et al., 2011). Orthopyroxene hydration established the retrograde anthophyllite-in isograd, which separates the hydrated zone from the granulite zone (Van Reenen, 1986). The hydrated zone occupies more than 4500 km^2 of crust in the hanging wall of the Hout River Shear Zone that bounds the SMZ in the south (Fig. 2) (e.g., Van Reenen et al., 2011).

3.1. Retrograde hydration: field observations and mineralogy

Cordierite hydration resulted in the formation of gedrite (comprising up to 2 wt.% Na_2O, Van Reenen, 1986) and kyanite. Hydration of cordierite (Fig. 3b) occurs over a wide area in the field that straddles the position of the anthophyllite-in isograd, indicating the divariant nature of the reaction. The hydration of cordierite can be expressed by the reaction (Van Reenen, 1986):

$$\underset{\text{Cordierite}}{5(Mg,Fe)_2Al_4Si_5O_{18}} + 2\,H_2O \rightarrow \underset{\text{Gedrite}}{2(Mg,Fe)_5Al_4Si_6O_{22}(OH)_2} + \underset{\text{Kyanite}}{6\,Al_2SiO_5} + \underset{\text{Quartz}}{7\,SiO_2} \quad (2)$$

which is probably not a completely true account of cordierite hydration as the Na_2O content of gedrite implies that a Na-bearing fluid phase was involved as a reactant. In the granulite zone, north of the anthophyllite-in isograd, hydration of cordierite is characterised by the inward growth of a fine-grained mixture of gedrite and kyanite at the cordierite edges and occurs while orthopyroxene remains stable (Fig. 3b). Cordierite hydration is most intense on and south of the anthophyllite-in isograd (Fig. 3c,d) where relatively coarse-grained gedrite-kyanite intergrowths pseudomorphically replace cordierite (Van Reenen, 1986). Cordierite hydration on the anthophyllite-in isograd is also associated with fine-grained euhedral garnet (Stevens, 1997), which is assumed to be related to the reaction:

$$\underset{\text{Gedrite}}{3(Mg,\ Fe)_5Al_4Si_6O_{22}(OH)_2} + 2\ K_2O + H_2O \rightarrow \underset{\text{Garnet}}{(Mg,Fe)_3Al_2Si_3O_{12}} + 4\ \underset{\text{Biotite}}{K(Mg,Fe)_3AlSi_3O_{10}(OH)_2} + 3\ \underset{\text{Kyanite}}{Al_2SiO_5} \quad (3)$$

Hydration of orthopyroxene (Fig. 3c), according to the reaction:

$$\underset{\text{Orthopyroxene}}{7/2(Mg,Fe)_2Si_2O_6} + \underset{\text{Quartz}}{SiO_2} + H_2O \rightarrow \underset{\text{Anthophyllite}}{(Mg,Fe)_7Si_8O_{22}(OH)_2} \quad (4)$$

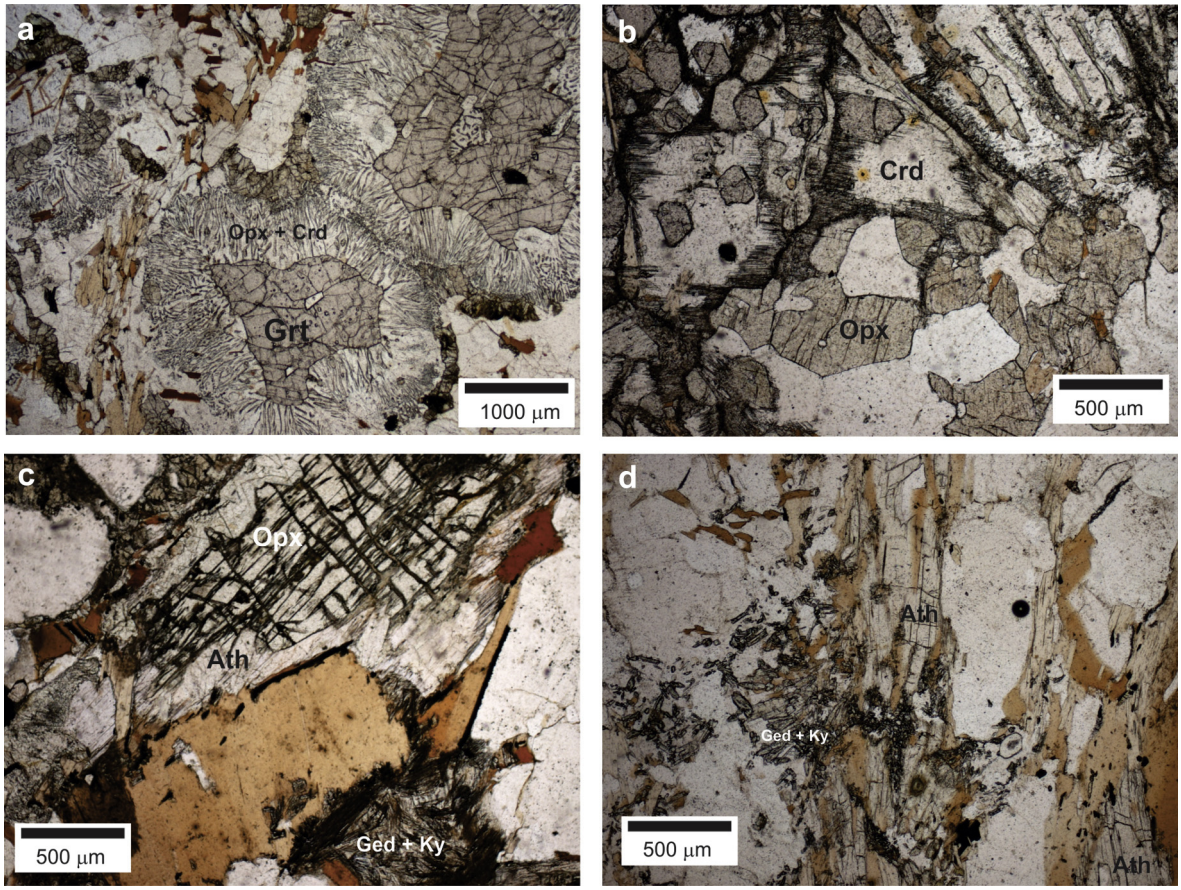

Figure 3. Microphotographs illustrating mineral assemblages and reaction textures in the SMZ. (a) Breakdown of garnet to form cordierite and orthopyroxene accruing to reaction (1). (b) Initial hydration of cordierite forming gedrite and kyanite (e.g., sample DR19, Fig. 2) according to reaction (2). Note that orthopyroxene is stable. (c) Initial hydration of orthopyroxene forming anthophyllite (e.g. sample DV157, Fig. 2) according to reaction (4). Note that cordierite has been completely replaced by gedrite and kyanite. (d) Complete hydration of cordierite and orthopyroxene (e.g., sample DV43). Mineral abbreviations are after Whitney and Evans (2010).

occurs within a few hundred meters in the field and defines the anthophyllite-in isograd. The isograd cuts through lithological boundaries and major fold structures (Van Reenen, 1986). The Mg/(Mg + Fe) mole ratio of 0.60–0.70 for both anthophyllite and orthopyroxene confirms the univariant nature of this reaction implying that the fluid phase was externally buffered (Van Reenen, 1986). It is important to note that graphite is commonly associated with the products of the reactions (2), (3), and (4) (Van Reenen, 1986; Stevens, 1997). South of the anthophyllite-in isograd, pelitic rocks comprise gedrite, kyanite (occasionally sillimanite), garnet, biotite, and anthophyllite (Fig. 3d) whereas orthopyroxene and cordierite are absent (Van Reenen, 1986).

3.2. Metasomatism

Metasomatic features in the hydrated zone of the SMZ are restricted to shear zones and include potassium alteration (Klipbank Shear Zone, Fig. 2) (Smit and Van Reenen, 1997) and lode-gold deposits (e.g., Louis Moore, Osprey and Doornhoek gold deposits, see Figs. 1 and 2) (Van Reenen et al., 1994). Shear zone hosted metasomatism of tonalitic gneisses at Klipbank is characterised by an increase in K_2O (from ~1.5 to ~4.5 wt.%) and decreasing MgO, FeO, CaO and TiO_2 whereas Al_2O_3 and SiO_2 remain constant (Mokgatlha, 1995; Smit and Van Reenen, 1997). Typically, the most altered rocks show coarse-grained microcline (replacing oligoclase), Mn-rich garnet, and sillimanite (Hoernes et al., 1995; Mokgatlha, 1995; Smit and Van Reenen, 1997). Lode-gold mineralisation is characterised by arsenopyrite, quartz veining, carbonate and potassium alteration (Van Reenen et al., 1994).

3.3. Fluid inclusions

Fluid inclusion studies on non-hydrated and hydrated granulites were performed by a number of workers including Van Reenen and Hollister (1988), Du Toit (1994), Mokgatlha (1995) and Van den Berg and Huizenga (2001) (Table 1). Van Reenen and Hollister (1988) studied both non-hydrated (north of the anthophyllite-in isograd) and hydrated (south of the anthophyllite-in isograd) granulites (sample localities: DR54, DR19, DR157, DV43, see Fig. 2). Du Toit (1994) and Van den Berg and Huizenga (2001) studied samples from two deep crustal shear zones (Petronella and Annaskraal Shear Zones, respectively) in the granulite zone (sample localities DT and VdB&H, see Fig. 2). Lastly, Mokgatlha (1995) studied samples from the Klipbank Shear Zone that is situated south of the isograd (sample locality: Mkg, Fig. 2). With the exception of the study by Van den Berg and Huizenga (2001), all fluid inclusion studies focussed on the

Table 1
Calculation results for $\log_{10} f_{O_2}^{fluid}$ assuming $X_{H_2O}/(X_{H_2O} + X_{CO_2} + X_{CH_4}) = 0.1,\ 0.3$ and $a_{carbon}^{fluid} = 1$ ($P = 6$ kbar, $T = 610$ °C). See text for discussion.

X_{H_2O}	$\log_{10} f_{O_2}^{fluid}$	$\log_{10} f_{O_2}^{fluid} - \log_{10} f_{O_2}^{FMQ}$	$X_{CO_2}/(X_{CO_2} + X_{CH_4})$
0.1	−18.9	+0.6	1
0.3	−19.0	+0.5	1

secondary (trail-bound) fluid inclusions only with inferences on either hydration and/or metasomatic processes that post-date the peak of metamorphism.

Microthermometry was performed on doubly polished thick sections (~200 μm) using a Chaixmeca (Van Reenen and Hollister, 1988), USGS (Du Toit, 1994; Mokgatlha, 1995), and Linkam heating-freezing stages (Van den Berg and Huizenga, 2001). The precision for the microthermometric measurements (<31 °C) is ~0.5 °C.

The above mentioned studies illustrate that both the granulites and the hydrated granulites have similar fluid inclusion assemblages. These include trail-bound CO_2-rich (Fig. 4a–c) and trail-bound aqueous inclusions with variable salinity.

3.3.1. CO_2-rich fluid inclusions

Melting of the CO_2-rich inclusions typically occurs near or at the triple point of pure CO_2 (−56.6 to −57.0 °C). Van den Berg and Huizenga (2001) reported on a few CO_2-rich inclusions in granulites north of the anthophyllite-in isograd that had significantly lower melting points (down to −58.5 °C) caused by the presence of CH_4 (up to ~10 mol.%). Although H_2O is not visible in the CO_2-rich fluid inclusions (Fig. 4a,b), it has in a few cases been detected by means of clathrate melting (Van Reenen and Hollister, 1988). This implies that the inclusions may contain up to 20 vol.% H_2O as this is optically not visible (e.g., Bakker and Diamond, 2006), particularly in small inclusions.

Homogenisation temperatures (*T*h) of CO_2-rich fluid inclusions are characterised by the disappearance of the vapour phase (liquid + vapour → liquid). Each trail typically shows a *T*h range of 10 °C or less. Van Reenen and Hollister (1988) identified relatively small and relatively low-density (*T*h = +12 to +26 °C) CO_2-rich fluid inclusions in short trails diverging from larger, higher density (*T*h = ~−4 °C) CO_2-rich fluid inclusions trails. Van den Berg and Huizenga (2001) described high-density trails of CO_2-rich fluid inclusions that are intersected by low-density CO_2-rich fluid inclusion trails (Fig. 4c). These textures show that the low-density inclusions formed later than the high-density ones. Further, it can be argued that some of the low-density inclusion trails were derived from decrepitated higher density CO_2-rich inclusions (Van Reenen and Hollister, 1988).

The *T*h bar plots show that all samples, hydrated or not, comprise low-density CO_2-rich fluid inclusions with a *T*h between +20 and +31 °C (Fig. 5a–g). Higher density inclusions (*T*h < +10 °C) are rarely present in the hydrated samples (Fig. 5e–g) whereas granulites north of the anthophyllite-in isograd contain inclusions with *T*h values as low as −30 °C (Fig. 5c).

3.3.2. Saline aqueous inclusions

Trails of aqueous inclusions have been described in all samples but are relatively rare. Therefore, a chronological relationship between the saline aqueous and the CO_2-rich trail-bound inclusions could not be established. In numerous aqueous inclusions salt cubes could be identified (Van Reenen and Hollister, 1988). Initial melting temperatures are variable with values as low as −55 °C, which indicates the presence of Ca^{2+} and Mg^{2+} in addition to Na^+ and probably K^+. Final ice melting temperatures range between −30 and 0 °C (Van Reenen and Hollister, 1988) indicating salinities ranging between ~30 and 0 wt.% NaCl equivalent.

3.4. P-T-fluid constraints on retrograde hydration and metasomatism in the SMZ

Oxygen-isotope thermometry of a rock sample that comprises cordierite without any sign of hydration (sample P19C, Venneman and Smith, 1992; Hoernes et al., 1995) points at an equilibrium temperature of ~670 °C. The orthopyroxene hydration temperature is calculated to be 610 °C from the garnet-biotite geothermometry (Kaneko and Miyano, 2004) using samples on the anthophyllite-in isograd comprising coexisting

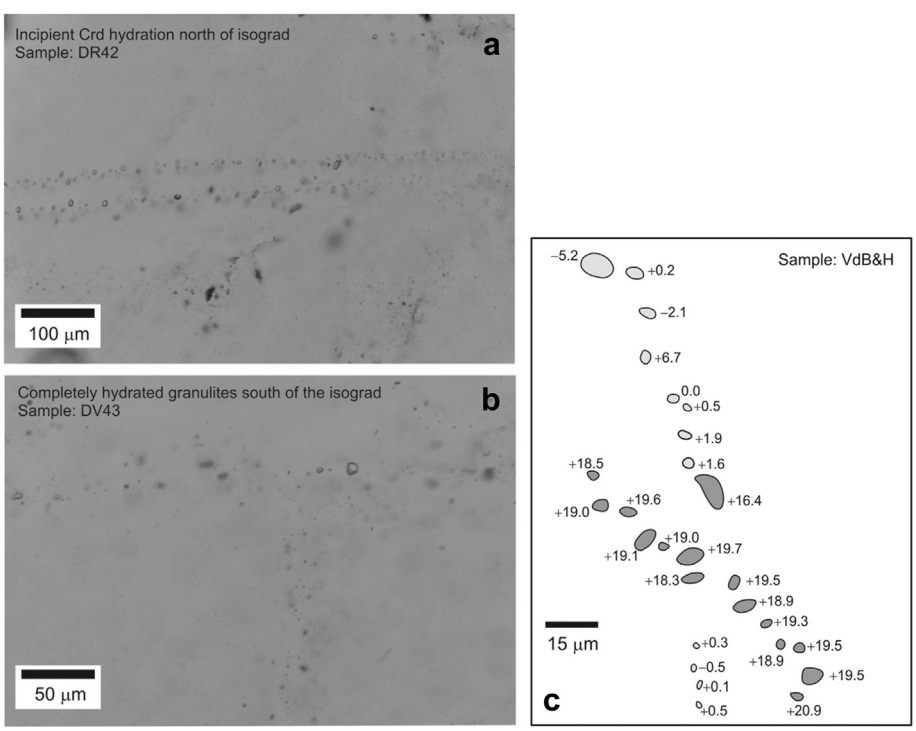

Figure 4. Microphotographs of fluid inclusion trails in quartz in initially (a) and completely (b) hydrated samples from the SMZ. (c) Illustration of high-density CO_2 fluid inclusion trail (light-grey inclusions) crosscut by a low-density CO_2 fluid inclusion trail (dark-grey inclusions), showing that low-density inclusions were formed after the high density ones (modified after Van den Berg and Huizenga, 2001). See Fig. 2 for sample localities.

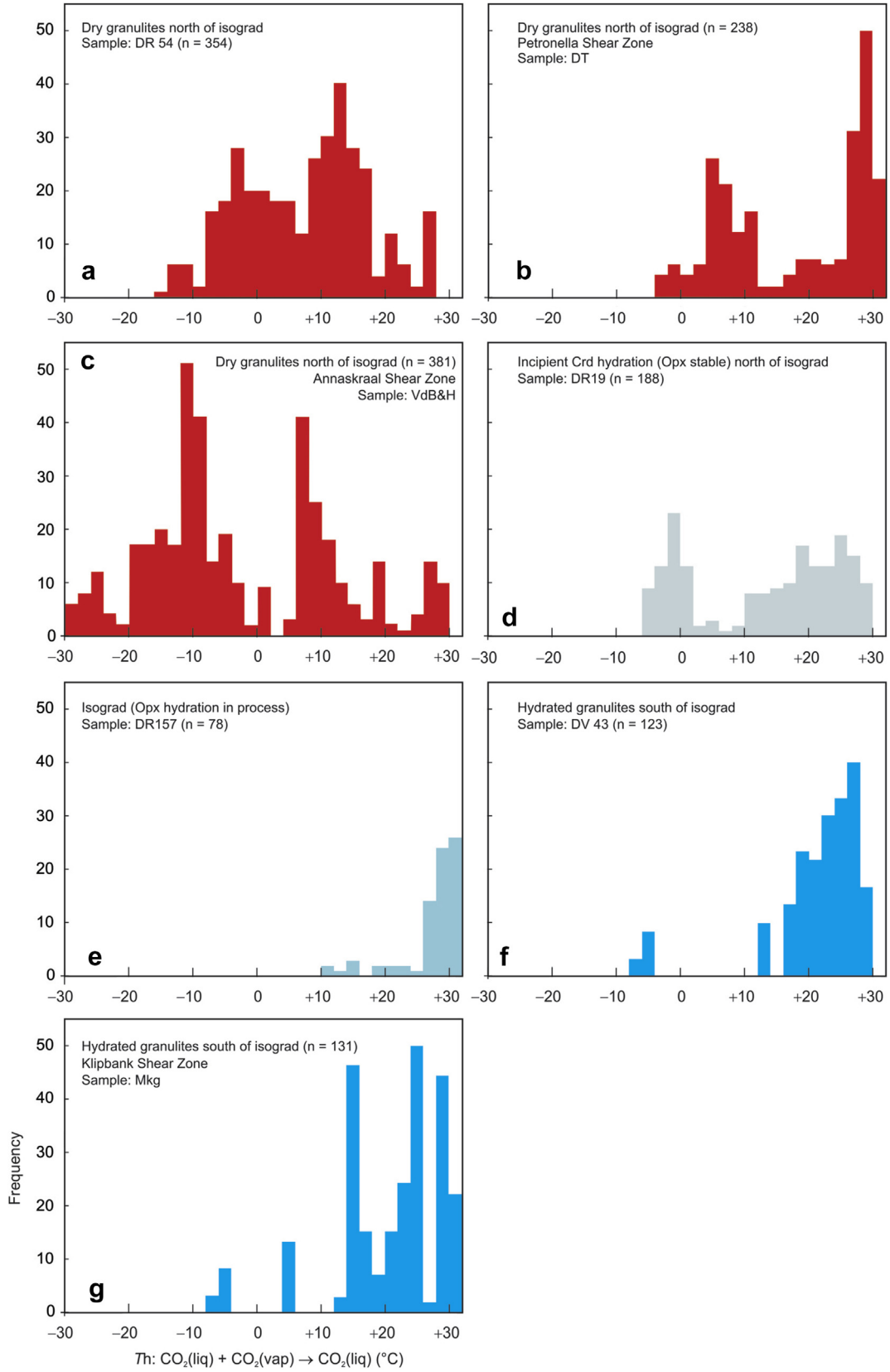

Figure 5. Bar plots (bar width is 2 °C) for *T*h for CO_2-rich trail-bound fluid inclusions measured in samples from different localities in the Southern Marginal Zone (see Fig. 2 for sample localities). Source of data: a, d–f: Van Reenen and Hollister (1988); b: Du Toit (1994); c: Van den Berg and Huizenga (2001); g: Mokgatlha (1995).

orthopyroxene and anthophyllite (Van Reenen, 1986). Whole-rock/mineral oxygen isotope fractionation of anthophyllite-bearing (orthopyroxene-absent) and metasomatized rocks (Klipbank Shear Zone) indicate fluid infiltration at ~600 °C (Hoernes et al., 1995). Based on the *P-T* path by Perchuk et al. (2000b) (Fig. 6), the pressure of orthopyroxene hydration should be slightly below 6 kbar rather than *at least* 6 kbar as previously suggested (Van Reenen, 1986).

So far, several authors have assumed that orthopyroxene hydration was caused by a low H_2O-activity fluid ($a^{fluid}_{H_2O}$ = ~0.2) (Van Reenen, 1986; Newton, 1994; Van Reenen et al., 2011). This is based on the fact that lowering $a^{fluid}_{H_2O}$ from unity to ~0.2 lowers the temperature for reaction (4) from ~800 to ~610 °C, assuming Mg end-members for both orthopyroxene and anthophyllite (Fig. 6) (Van Reenen, 1986; Newton, 1994; Van Reenen et al., 2011). However, orthopyroxene and anthophyllite do comprise significant amounts of Fe (Van Reenen, 1986). Using the Wood and Banno (1973) orthopyroxene activity-composition model and the orthopyroxene compositions from Van Reenen (1986), the average enstatite activity in orthopyroxene is ~0.39. Evaluation of the orthopyroxene hydration reaction using the spreadsheet PTGibbs (Brandelik and Massonne, 2004) in conjunction with Holland and Powell's (1998) dataset shows that the Fe content in anthophyllite and $a^{fluid}_{H_2O}$ have opposite effects on the temperature of reaction (4). An increase in the Fe content of anthophyllite can be compensated by an increase of $a^{fluid}_{H_2O}$ (i.e., greater than 0.2) in order to maintain the temperature of orthopyroxene hydration at 610 °C. Therefore, $a^{fluid}_{H_2O}$ of ~0.2 represents a minimum value for the hydrating fluid.

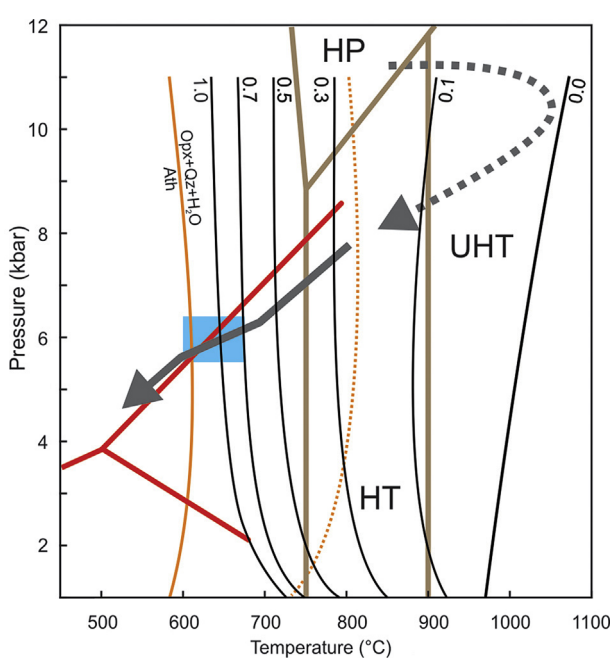

Figure 6. Pressure-temperature diagram illustrating the partial prograde and retrograde *P-T* paths of the Southern Marginal Zone, and the *P-T* conditions for the cordierite and orthopyroxene hydration reactions (blue box). Solidus curves (Qz-Ab-Or-H_2O-CO_2 system) labelled for different X_{H_2O} values are indicated (black curves) (Ebadi and Johannes, 1991). The dashed *P-T* loop is after Belyanin et al. (2012) (see Fig. 2 for sample locality). The retrograde *P-T* path (solid grey arrow) is the average for samples DR19, DV101 and DV3 (see Fig. 2 for sample localities) as calculated by Perchuk et al. (2000b). The orange curves represent the enstatite-anthophyllite (Mg end-members) stability curve for a $a^{fluid}_{H_2O}$ of 1 (dashed curve) and 0.2 (solid curve). The subdivision of the granulite facies into different *P-T* regimes is after Brown (2007): HT = high temperature; UHT = ultrahigh temperature; HP = high pressure. The Al-silicate system (red curves) is after Holdaway (1971).

There is little doubt that the low $a^{fluid}_{H_2O}$ fluid in the SMZ is a carbon-saturated CO_2-rich fluid. Evidence for this includes: (1) the occurrence of graphite associated with the hydration reaction products, (2) carbonation reactions that occur in ultramafic rocks in the hydrated part of the SMZ, i.e. the transformation of olivine into magnesite and orthopyroxene according to the reaction olivine + CO_2 → orthopyroxene + magnesite (Van Schalkwyk and Van Reenen, 1992), and (3) the presence of secondary CO_2-rich fluid inclusion trails.

The minimum $a^{fluid}_{H_2O}$ value of ~0.2 corresponds to a minimum X_{H_2O} value of ~0.1 in a CO_2-rich fluid (Aranovich and Newton, 1996). The upper X_{H_2O} limit in a CO_2-rich fluid can be established from the lower temperature limit of melting at ~800 °C (Smit and Van Reenen, 1997). This temperature corresponds with the solidus (Qz-Ab-Or-H_2O-CO_2 system) for X_{H_2O} = ~0.3 (Fig. 6), i.e. X_{H_2O} was ≤0.3. Therefore, X_{H_2O} of the hydrating fluid in the SMZ ranged between 0.1 and 0.3, which is in good agreement with the observed CO_2-rich fluid inclusions without any visible H_2O. Using the software by Bakker (2003) (i.e., BULK), X_{H_2O} values of 0.1 and 0.3 correspond to a water volume fractions of <~5 and <~15 vol.%, respectively, which is hardly visible.

The temperature of metasomatism in the Klipbank Shear Zone was determined from whole-rock/Grt/Qz oxygen-isotope fractionation and found to be ~600 °C (Hoernes et al., 1995). This temperature has also been established for gold mineralisation based on the alteration assemblage (Van Reenen et al., 1994). The alkali mobility exemplified by metasomatism requires the presence of a saline fluid in addition to the CO_2-rich fluid. The secondary trail-bound saline aqueous fluid inclusions may represent this fluid. Considering the variation in the salt content of these fluids, it is likely that the fluid trapped in these inclusions resulted from mixing between two fluids with contrasting salinities (e.g., Wilkinson, 2001). In that case, the fluid inclusions with the highest salinity (i.e., ~30 wt.% NaCl equivalent) represent the saline aqueous fluid that is responsible for potassium alteration and gold mineralisation whereas the low-salinity fluid is probably meteoric in origin (e.g., Yardley et al., 2000).

4. C-O-H fluid modelling

4.1. Equilibrium calculations

In this study, C-O-H model calculations are used to constrain the redox state of the fluid-rock system, and for testing whether fluid inclusion data and fluid compositions determined from metamorphic reactions are in agreement. Aspects of C-O-H fluid calculations have been addressed by numerous authors (French, 1966; Ohmoto and Kerrick, 1977; Huizenga, 2001 and references therein). A C-O-H fluid system has seven unknowns at a fixed fluid pressure and temperature: X_{H_2O}, X_{CO_2}, X_{CH_4}, X_{H_2}, X_{CO}, $f^{fluid}_{O_2}$, and a^{fluid}_{carbon}, i.e. the mole fractions of H_2O, CO_2, CH_4, H_2, CO, the fluid oxygen fugacity and the fluid carbon activity, respectively. Four independent equilibria can be written (e.g., French, 1966; Ohmoto and Kerrick, 1977) for the C-O-H fluid system: $CO + ½\ O_2 \Leftrightarrow CO_2$, $H_2 + ½\ O_2 \Leftrightarrow H_2O$, $CH_4 + 2\ O_2 \Leftrightarrow CO_2 + 2H_2O$, and $C + O_2 \Leftrightarrow CO_2$. The mass balance constraint yields (ignoring the very small value of X_{O_2}) $X_{H_2O} + X_{CO_2} + X_{CH_4} + X_{CO} + X_{H_2} = 1$. Having defined five equations for the C-O-H system, two compositional parameters need to be specified in order to calculate the remaining five variables. One can choose any two compositional parameters (e.g., single mole fractions, mole fraction ratio's, atomic ratio's, a fixed a^{fluid}_{carbon} of 1 if graphite is present, see Huizenga, 2001) to solve this system. However, the choice of these two parameters obviously depends on what data are available.

We used the following constraints for the calculations: (1) P and T conditions were set at 6 kbar and 610 °C, respectively, (2) a^{fluid}_{carbon} was set at unity assuming carbon saturation ($a^{fluid}_{carbon} = 1$), and (3) the $X_{H_2O}/(X_{H_2O} + X_{CO_2} + X_{CH_4})$ ratio was set 0.1/0.3. The first constraint is based on the P-T hydration conditions of orthopyroxene. The second constraint is based on the presence of graphite associated with the hydration reaction products. The last constraint is in accordance with the estimated X_{H_2O} ranging between 0.1 and 0.3, which corresponds to a similar $X_{H_2O}/(X_{H_2O} + X_{CO_2} + X_{CH_4})$ ratio assuming that both X_{H_2} and X_{CO} occur in negligible amounts. These three constraints make the C-O-H system invariant allowing the calculation of $f^{fluid}_{O_2}$ and $X_{CO_2}/(X_{CO_2} + X_{CO_4})$.

An updated version of the spreadsheet COH (Huizenga, 2005) was used to perform the calculations. Thermodynamic data for the fluid species and graphite for calculating equilibrium constants for reactions in the fluid phase were taken from Holland and Powell (1998). Fugacity coefficients for the fluid species were calculated from the equations of state by Shi and Saxena (1992) assuming ideal mixing. Note that the calculated results for $f^{fluid}_{O_2}$ are reported as absolute values and as values relative to f_{O_2} buffered by the fayalite-magnetite-quartz (FMQ) buffer ($f^{FMQ}_{O_2}$) calculated from the equation (Ohmoto and Kerrick, 1977): $\log_{10} f^{FMQ}_{O_2} = -25738/T + 9.00 + 0.092(P-1)/T$ (T in kelvin, P in atmosphere).

4.2. Results

The calculation results (Table 1) show that the $\log_{10} f^{fluid}_{O_2}$ is 0.5–0.6 $\log_{10}$ units higher than $\log_{10} f^{FMQ}_{O_2}$. The calculations also show that $X_{CO_2}/(X_{CO_2} + X_{CH_4})$ is 1, which is generally in good agreement with melting temperatures of most of the CO_2-rich fluid inclusions near triple point of CO_2. However, the melting point of some of these inclusions below the triple point of CO_2 (i.e., ~−57 °C) is most likely due to some CH_4 (up to 5 mol.%, Thiéry et al., 1994) as graphite is present in the hydrated rocks. The calculated $X_{CO_2}/(X_{CO_2} + X_{CH_4})$ value of 1 indicates that CH_4 was not a primary species in the CO_2-rich fluid but resulted from post-trapping changes (Hall and Bodnar, 1990).

In order to confirm the secondary origin of CH_4 in the CO_2-rich fluid another calculation was done using a different compositional constraint. Instead of defining $X_{H_2O}/(X_{H_2O} + X_{CO_2} + X_{CH_4})$ we fixed $X_{CO_2}/(X_{CO_2} + X_{CH_4})$ at 0.99/0.95 (Table 2), allowing the calculation of $X_{H_2O}/(X_{H_2O} + X_{CO_2} + X_{CH_4})$ and $f^{fluid}_{O_2}$. The calculated $X_{H_2O}/(X_{H_2O} + X_{CO_2} + X_{CH_4})$ can be compared with the X_{H_2O} of the CO_2-rich fluid (i.e., between 0.1 and 0.3). The results show that a fluid with $X_{CO_2}/(X_{CO_2} + X_{CH_4})$ between 0.99 and 0.95 should have had a $X_{H_2O}/(X_{H_2O} + X_{CO_2} + X_{CH_4})$ value between 0.6 and 0.8, respectively and $f^{fluid}_{O_2}$ near FMQ (Table 2). This result is unrealistic as the relatively high X_{H_2O} value implies that orthopyroxene hydration would have occurred at a temperature higher than 610 °C. Therefore, the presence of CH_4 in the CO_2-rich inclusions can only be explained by H_2 diffusion into the inclusions (Hall and Bodnar, 1990).

Summarising, the C-O-H calculations demonstrate that: (1) the presence of carbon-saturated CO_2-rich fluids requires a $f^{fluid}_{O_2}$ that is 0.5–0.6 $\log_{10}$ units above FMQ and (2) the carbonic component was pure CO_2.

Table 2
Calculation results for $X_{H_2O}/(X_{H_2O} + X_{CO_2} + X_{CH_4})$ and $\log_{10} f^{fluid}_{O_2}$ assuming $X_{CO_2}/(X_{CO_2} + X_{CH_4}) = 0.99$, 0.95 and $a^{fluid}_{carbon} = 1$ ($P = 6$ kbar, $T = 610$ °C). See text for discussion.

$X_{CO_2}/(X_{CO_2} + X_{CH_4})$	$\log_{10} f^{fluid}_{O_2}$	$\log_{10} f^{fluid}_{O_2} - \log_{10} f^{FMQ}_{O_2}$	$X_{H_2O}/(X_{H_2O} + X_{CO_2} + X_{CH_4})$
0.99	−19.3	+0.2	0.62
0.95	−19.6	0.0	0.78

5. Discussion and conclusions

5.1. Source of the CO_2-rich and saline aqueous fluids

Both CO_2-rich and aqueous saline aqueous fluids (~30 wt.% NaCl equivalent) infiltrated the granulites during cooling at P-T of hydration 6 kbar and 610 °C, respectively. This is illustrated by (1) the occurrence of anthophyllite, gedrite, kyanite and graphite, (2) the involvement of Na and K in reactions (2) and (3), respectively, (3) shear zone hosted metasomatism (Klipbank Shear Zone), and (4) the presence of CO_2-rich and saline aqueous fluid inclusion trails. The pervasive nature of fluid infiltration is inferred from the widespread occurrence of the hydrated mineral phases. Whole-rock/mineral oxygen isotope fractionation patterns indicate an external fluid source (Hoernes et al., 1995). Although there is no direct fluid inclusion evidence, it is likely that both fluids were immiscible.

Two potential sources for the CO_2-rich fluid have been suggested in previous studies, namely devolatilization reactions within the underlying greenstone belt rocks (Van Reenen and Hollister, 1988) and a deep mantle source (Van Reenen et al., 1994). A mantle source was suggested based on the $\delta^{13}C$ signature (−5 to −6‰) of magnesite in hydrated ultramafic rocks (Van Schalkwyk and Van Reenen, 1992). However, these values do not conclusively point to a mantle source (Kerrich, 1987). Therefore, prograde devolatilization reactions in the underlying greenstone belt rocks from the Kaapvaal Craton footwall are the most plausible source for CO_2-rich fluids. This is supported by the fact that underthrusted mica schist from the Sutherland/Giyani greenstone belt (Fig. 1) reached peak P-T conditions (~600 °C and 5–5.5 kbar, Fig. 7) (Perchuk et al., 2000a) at ~2.69 Ga (Kreissig et al., 2001), which is contemporaneous with the early stage of SMZ exhumation

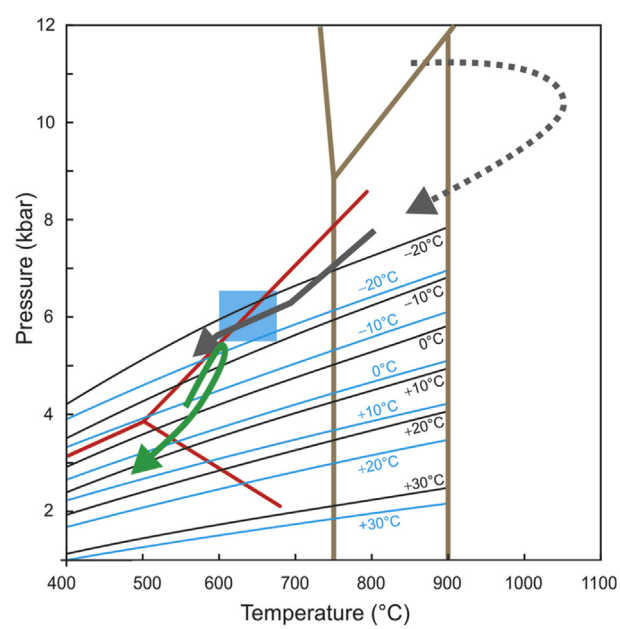

Figure 7. Pressure-temperature diagram illustrating the retrograde P-T path of the Southern Marginal Zone (grey arrow, see Fig. 6) and the P-T loop for the Sutherland/Giyani greenstone belt (green arrow, see Fig. 1 for locality of Sutherland/Giyani greenstone belt) (Perchuk et al., 2000a). Granulite fields and the Al-silicate system are the same as in Fig. 6. Blue box: P-T conditions for hydration of cordierite and orthopyroxene. Grey lines represent isochores for CO_2-rich fluid inclusions (black lines: $X_{H_2O} = 0.3$, blue lines $X_{H_2O} = 0.1$) for different Th values. Isochores were calculated from the equation of state by Bakker (1999) using the program *Isochore* (Bakker, 2003). Blue box indicates the P-T conditions for cordierite and orthopyroxene hydration.

Table 3
Molar volumes of products and reactants, and volume change (solid phases) of reactions in the SMZ calculated using Holland and Powell's (1998) dataset ($P = 5–7$ kbar, $T = 600–700$ °C).

Reaction	Reaction no. in text	$V_{products}$ (cm^3/mol)	$V_{reactants}$ (cm^3/mol)	$\Delta_r V_{solids}$ (%)
5 Mg-Crd + 2H_2O → 2 Ged + 6 Ky + 7 Qz	2	967	1155	−19
3 Ged + 2 K_2O (fluid) + H_2O → Grt + 4 Bt + 3 Ky	3	853	767	+9
3.5 En + Qz + H_2O → Ath	4	263	241	+9
3.5Fs + Qz + H_2O → Fe-Ath	4	280	260	+8

(Kreissig et al., 2001). In other words, prograde metamorphism in footwall greenstone belts is caused by thrusting of SMZ granulites over the Kaapvaal Craton along the bounding Hout River Shear Zone (e.g., Roering et al., 1992; Van Reenen et al., 2011). Greenstone belt fluids produced during prograde metamorphism are typically aqueous-carbonic in composition (Powell et al., 1991). This fluid may become CO_2 rich if (1) $T > 500$ °C (Powell et al., 1991), (2) the greenstone belt is dominated by (ultra)mafic lithologies (Powell et al., 1991), or (3) the fluid interacts with graphite in a relatively oxidised environment.

The source of the saline aqueous fluid remains hypothetical. It could either be inherited from granulites, or derived from underlying greenstone belts. Greenstone belts are known to contain evaporitic brines (e.g. Westall et al., 2002) and connate saline waters (Glassly et al., 2010).

5.2. Fluid-rock redox state during hydration

The oxygen fugacity of the CO_2-rich fluid is 0.5–0.6 $\log_{10}$ units higher than $f_{O_2}^{FMQ}$. The pervasive nature of fluid infiltration implies that the fluid phase and host-rock were in redox equilibrium (i.e., $f_{O_2}^{fluid} = f_{O_2}^{rock}$). Considering the fact that graphite is part of the hydration mineral assemblages, oxidation of the host rocks must have occurred during retrograde hydration as a result of graphite precipitation according to the reaction $CO_2 \rightarrow C + O_2$. In other words, graphite precipitation was driven by the redox difference of the oxidised and the relatively reduced host rock and redox equilibrium was reached during graphite precipitation (e.g., Huizenga and Touret, 2012). Local redox variations (i.e., more oxidised) in the host rock explain the absence of graphite in some of the hydrated rocks.

5.3. Fluid migration in the lower and middle crust

Whereas a saline aqueous fluid is highly mobile, a CO_2-rich fluid is considered to be immobile in the continental crust because of its wetting angle characteristics (Watson and Brennan, 1987). Flow of the CO_2-rich fluid along grain boundaries is, therefore, not feasible. Other factors must have played a role such as fluid flow along deep- to mid-crustal shear zones, volume changes associated with hydration reactions, and fluid-induced micro fracturing.

Firstly, the relatively high spatial density of shear zones south of the isograd compared to the northern part is noteworthy (Fig. 2) and indicates a structural control on the fluid flow. In particular strike slip faults, where the fluid pressure is expected to be less than the lithostatic pressure, will be preferred sites for focussed fluid flow (Roering et al., 1995).

Second, volume changes associated with retrograde hydration reactions in the SMZ were significant (Table 3) and did probably contribute to an increase in the permeability of the rocks (e.g., Jamtveit, 2010). A volume increase (i.e., reactions (3) and (4), Table 3) may cause fracturing whereas a volume decrease associated with the replacement of cordierite by gedrite, kyanite and quartz (reaction (2), Table 3) will cause an increase in the porosity. In both cases, the permeability of the rocks will increase (e.g., Oliver, 1996; Putnis, 2009; Putnis and Austrheim, 2013).

Another possible driving force for fluid flow includes grain-size scale porosity (e.g., Oliver, 1996) as exemplified by trails comprising CO_2-rich fluid inclusions. Here, permeability is created by overpressured fluids causing micro-hydrofracturing (e.g., Touret and Huizenga, 2012). Considering the relatively flat slope of isochores for CO_2-rich fluids in *P-T* space, hydrofracturing is only possible if the retrograde *P-T* path is dominated by decompression rather than cooling. So, in the case for the SMZ, this mechanism is not relevant for cooling between 800 and 600 °C where the retrograde *P-T* path is approximately parallel to the isochores for the CO_2-rich fluids (Fig. 7).

The expected *T*h range for CO_2-rich fluid inclusions, which are trapped during retrograde hydration (between ~670 and ~600 °C), is between −20 and −10 °C (Fig. 7). However, such CO_2-rich fluid inclusions have not been found (Fig. 5d–g). The relatively low density of the CO_2-rich inclusions can be explained by (1) the fact that some of the low-density inclusions comprise the CO_2-rich fluid that was liberated from originally higher density CO_2 fluid inclusions that decrepitated during decompression (Van Reenen and Hollister, 1988), and (2) trapping of the fluid at a pressure between the lithostatic and hydrostatic pressure. The latter is expected to occur in a strike slip environment as mentioned above (Roering et al., 1995) and also there where hydration reactions have increased the permeability of the rocks.

Acknowledgements

We would like to thank D. Harlov and M. Santosh for the opportunity to write this paper. Thorough reviews by Leonid Aranovich and Fons van den Kerkhof have improved the paper significantly. DDvR would like to thank the NRF (Grant No. IFR1202190048) and the University of Johannesburg for financial support.

References

Aranovich, L.Ya., Newton, R.C., 1996. H_2O activity in concentrated NaCl solutions at high pressures and temperatures measured by the brucite–periclase equilibrium. Contributions to Mineralogy and Petrology 125, 200–212.
Bakker, R.J., 1999. Adaptation of the Bowers and Helgeson (1983) equation of state to the H_2O-CO_2-CH_4-N_2-NaCl system. Chemical Geology 154, 225–236.
Bakker, R.J., 2003. Package FLUIDS 1. Computer programs for analysis of fluid inclusion data and for modelling bulk fluid properties. Chemical Geology 194, 3–23.
Bakker, R.J., Diamond, L.W., 2006. Estimation of volume fractions of liquid and vapor phases in fluid inclusions, and definition of inclusion shapes. American Mineralogist 91, 635–657.
Belyanin, G.A., Rajesh, H.M., Sajeev, K., Van Reenen, D.D., 2012. Ultrahigh-temperature metamorphism from an unusual corundum + orthopyroxene intergrowth bearing Al–Mg granulite from the Southern Marginal Zone, Limpopo Complex, South Africa. Contributions to Mineralogy and Petrology 164, 457–475.
Brandelik, A., Massonne, H.-J., 2004. PTGIBBS—an EXCEL™ Visual Basic program for computing and visualizing thermodynamic functions and equilibria of rock-forming minerals. Computers & Geosciences 30, 909–923.
Brown, M., 2007. Metamorphic conditions in orogenic belts: a record of secular change. International Geology Review 49, 193–234.

Du Toit, R., 1994. High-temperature Metasomatic Alteration Associated with Deep Crustal Shear Zones in the Limpopo Belt, South Africa. Unpublished MSc Thesis. Rand Afrikaans University (now University of Johannesburg), p. 304.
Ebadi, A., Johannes, W., 1991. Beginning of melting and composition of first melts in the system Qz-Ab-Or-H_2O-CO_2. Contributions Mineralogy Petrology 106, 286–295.
French, B.M., 1966. Some geological implications of equilibrium between graphite and a C-O-H gas at high temperatures and pressures. Reviews in Geophysics 4, 223–253.
Glassly, W.E., Kortgård, J.A., Sørensen, K., 2010. K-rich brine and chemical modification of the crust during continent-continent collision, Nagssugtoqidian Orogen, West Greenland. Precambrian Research 180, 47–62.
Holland, T.J.B., Powell, R., 1998. An internally consistent thermodynamic data set for phases of petrological interest. Journal of Metamorphic Geology 16, 309–343.
Hall, D.L., Bodnar, R.J., 1990. Methane in fluid inclusions from granulites: a product of hydrogen diffusion? Geochimica et Cosmochimica Acta 54, 641–651.
Hoernes, S., Lichtenstein, U., Van Reenen, D.D., Mokgatlha, K., 1995. Whole-rock/mineral O-isotope fractionations as a tool to model fluid-rock interaction in deep seated shear zones of the Southern Marginal Zone of the Limpopo Belt, South Africa. South African Journal of Geology 98, 488–497.
Holdaway, M.J., 1971. Stability of andalusite and the aluminium silicate phase diagram. American Journal of Science 271, 91–131.
Huizenga, J.M., 2001. Thermodynamic modelling of C-O-H fluids. Lithos 55, 101–114.
Huizenga, J.M., 2005. COH, an Excel spreadsheet for composition calculations in the C-O-H fluid system. Computers & Geoscience 31, 797–800.
Huizenga, J.M., Touret, J.L.R., 2012. Granulites, CO_2 and graphite. Gondwana Research 22, 799–809.
Jamtveit, B., 2010. Metamorphism: from patterns to processes. Elements 6, 149–152.
Kaneko, Y., Miyano, T., 2004. Recalibration of mutually consistent garnet-biotite and garnet-cordierite geothermometers. Lithos 73, 255–269.
Kerrich, R., 1987. The stable isotope geochemistry of Au-Ag vein deposits in metamorphic rocks. In: Kyser, T.K. (Ed.), Stable Isotope Geochemistry of Low Temperature Fluids. Mineralogical Association of Canada Short Course Handbook, vol. 13, pp. 287–336.
Kreissig, K., Nägler, T.F., Kramers, J.D., Van Reenen, D.A., Smit, C.A., 2000. An isotopic and geochemical study of the northern Kaapvaal craton and the Southern marginal zone of the Limpopo Belt: are they juxtaposed terranes? Lithos 50, 1–25.
Kreissig, K., Holzer, L., Frei, R., Villa, I.M., Kramers, J.D., Kröner, A., Smit, C.A., Van Reenen, D.D., 2001. Geochronology of the Hout River Shear Zone and the metamorphism in the Southern Marginal Zone of the Limpopo Belt, Southern Africa. Precambrian Research 109, 145–173.
Mokgatlha, K.B.G., 1995. The Transformation of Tonalitic Gneiss into Potassic Garnet-sillimanite Gneiss in a Deep Crustal Shear Zone in the Limpopo Belt. Unpublished MSc Thesis. Rand Afrikaans University (now University of Johannesburg), p. 163.
Newton, R.C., 1994. Simple-system mineral reactions and high-grade metamorphic fluids. European Journal of Mineralogy 7, 861–881.
Newton, R.C., Aranovich, L.Ya., Hansen, E.C., Vandenheuvel, B.A., 1998. Hypersaline fluids in deep-crustal metamorphism. Precambrian Research 91, 41–63.
Ohmoto, H., Kerrick, D., 1977. Devolatilization equilibria in graphitic systems. American Journal of Science 277, 1013–1044.
Oliver, N.H.S., 1996. Review and classification of structural controls on fluid flow during regional metamorphism. Journal of Metamorphic Geology 14, 477–492.
Perchuk, L.L., Gerya, T.V., Van Reenen, D.D., Smit, C.A., Krotov, A.V., 2000a. *P-T* paths and tectonic evolution of shear zones separating high-grade terrains from cratons: examples from Kola Peninsula (Russia) and Limpopo Region (South Africa). Mineralogy and Petrology 69, 109–142.
Perchuk, L.L., Gerya, T.V., Van Reenen, D.D., Krotov, A.V., Safanov, O.G., Smit, C.A., Shur, M.Y., 2000b. Comparable petrology and metamorphic evolution of the Limpopo (South Africa) and Lapland (Fennoscandia) high-grade terrains. Mineralogy and Petrology 69, 69–107.
Powell, R., Will, T.M., Phillips, G.N., 1991. Metamorphism in Archaean greenstone belts: calculated fluid compositions and implications for gold mineralization. Journal of Metamorphic Geology 9, 141–150.
Putnis, A., 2009. Mineral replacement reactions. In: Oelkers, E.H., Schott, J. (Eds.), Thermodynamics and Kinetics of Water-rock Interaction. Mineralogical Society of America, Reviews in Mineralogy & Geochemistry, vol. 70, pp. 87–124.
Putnis, A., Austrheim, H., 2013. Mechanisms of metasomatism and metamorphism on the local mineral scale: the role of dissolution-reprecipitation during mineral re-equilibration. In: Harlov, D., Austrheim, H. (Eds.), Metasomatism and the Chemical Transformation of Rock. The Role of Fluids in Terrestrial and Extraterrestrial Processes. Lecture Notes in Earth System Sciences, pp. 141–170.
Roering, C., Van Reenen, D.D., Smit, C.A., Du Toit, R., 1995. Deep crustal embrittlement and fluid flow during granulite metamorphism in the Limpopo Belt, South Africa. Journal of Geology 103, 673–686.
Roering, C., Van Reenen, D.D., Smit, C.A., Barton Jr., J.M., De Beer, J.H., De Wit, M.J., Stettler, E.H., Van Schalkwyk, J.F., Stevens, G., Pretorius, S., 1992. Tectonic model for the evolution of the Limpopo Belt. Precambrian Research 55, 539–552.
Rollinson, H.R., 1993. A terrane interpretation of the Archaean Limpopo Belt. Geological Magazine 130, 755–765.
Shi, P., Saxena, S.K., 1992. Thermodynamic modelling of the C-O-H-S fluid system. American Mineralogist 77, 1038–1049.
Smit, C.A., Van Reenen, D.D., 1997. Deep crustal shear zones, high-grade tectonites, and associated metasomatic alteration in the Limpopo Belt, South Africa: Implications for deep crustal processes. Journal of Geology 105, 37–57.
Stevens, G., 1997. Melting, carbonic fluids and water recycling in the deep crust: an example from the Limpopo Belt, South Africa. Journal of Metamorphic Geology 15, 141–154.
Thiéry, R., Van den Kerkhof, A.M., Dubessy, J., 1994. *vX* properties of CH_4-CO_2 and CO_2-N_2 fluid inclusions: modelling for $T < 31$ °C and $P < 400$ bars. European Journal of Mineralogy 6, 753–772.
Touret, J.L.R., Huizenga, J.M., 2011. Fluids in granulites. In: van Reenen, D.D., Kramers, J.D., McCourt, S., Perchuk, L.L. (Eds.), Origin and Evolution of Precambrian High-grade Gneiss Terranes, With Special Emphasis on the Limpopo Complex of Southern Africa. Geological Society of America Memoir, vol. 207, pp. 25–37.
Touret, J.L.R., Huizenga, J.M., 2012. Fluid-assisted granulite metamorphism: a continental journey. Gondwana Research 21, 224–235.
Tsunogae, T., Miyano, T., Van Reenen, D.D., Smit, C.A., 2004. Ultrahigh-temperature metamorphism of the Southern Marginal Zone of the Archean Limpopo Belt. South Africa: Journal of Mineralogical and Petrological Sciences 99, 213–224.
Van den Berg, R., Huizenga, J.M., 2001. Fluids in granulites of the Southern Marginal Zone of the Limpopo Belt. Contributions to Mineralogy and Petrology 141, 529–545.
Van Reenen, D.D., 1986. Hydration of cordierite and hypersthene and a description of the retrograde orthoamphibole isograd in the Limpopo Belt, South Africa. American Mineralogist 71, 900–915.
Van Reenen, D.D., Hollister, L.S., 1988. Fluid inclusions in hydrated granulite facies rocks, Southern Marginal Zone of the Limpopo Belt, South Africa. Geochimica et Cosmochica Acta 52, 1057–1064.
Van Reenen, D.D., Pretorius, A.I., Roering, C., 1994. Characterization of fluids associated with gold mineralisation and with regional high-temperature retrogression of granulites in the Limpopo Belt, South Africa. Geochimica et Cosmochimica Acta 58, 1147–1159.
Van Reenen, D.D., Perchuk, L.D., Roering, C., Boshoff, R., 2011. Thrust exhumation of the Neoarchean ultrahigh-temperature Southern Marginal Zone, Limpopo Complex: convergence of decompression-cooling paths in the hanging wall and prograde P-T paths in the footwall. In: Van Reenen, D.D., Kramers, J.D., McCourt, S., Perchuk, L.L. (Eds.), Origin and Evolution of Precambrian High-grade Gneiss Terranes, With Special Emphasis on the Limpopo Complex of Southern Africa. Geological Society of America Memoir, vol. 207, pp. 189–212.
Van Schalkwyk, J.F., Van Reenen, D.D., 1992. High-temperature hydration of ultramafic granulites from the Southern Marginal Zone of the Limpopo Belt by infiltration of CO_2-rich fluid. Precambrian Research 55, 337–352.
Venneman, T.W., Smith, H.S., 1992. Stable isotope profile across the orthoamphibole isograd in the Southern Marginal Zone of the Limpopo Belt, South Africa. Precambrian Research 55, 365–397.
Watson, E.B., Brennan, J.M., 1987. Fluids in the lithosphere 1. Experimentally determined wetting characteristics of CO_2-H_2O fluids and their implication for fluid transport, host-rock physical properties and fluid inclusion formation. Earth and Planetary Science Letters 85, 497–515.
Westall, F., De Wit, M.J., Dann, J., Van der Gaast, S., De Ronde, C.E.J., Gerneke, D., 2002. Early Archean fossil bacteria and biofilms in hydrothermally-influenced sediments from the Barberton greenstone belt, South Africa. Precambrian Research 106, 93–116.
Whitney, D.L., Evans, B.W., 2010. Abbreviations for names of rock-forming minerals. American Mineralogist 95, 185–187.
Wilkinson, J.J., 2001. Fluid inclusions in hydrothermal ore deposits. Lithos 55, 229–272.
Wood, B.J., Banno, S., 1973. Garnet-orthopyroxene and orthopyroxene-clinopyroxene relationships in simple and complex systems. Contributions to Mineralogy and Petrology 42, 109–124.
Yardley, B., Gleeson, S., Bruce, S., Banks, D., 2000. Origin of retrograde fluids in metamorphic rocks. Journal of Geochemical Exploration 69–70, 281–285.